SUBCONTRACT TITLE**:** **Fabrication and Physics of CdTe Devices by Sputtering**

SUBCONTRACT TITLE**:** **RXL-5-44205-01**

QUARTERLY TECHNICAL STATUS REPORT FOR**:**

Phase 3/Quarter 2

SUBMITTED TO**:** **Bolko von Roedern**
National Renewable Energy Laboratory

PRINCIPAL INVESTIGATORS:

A.D. Compaan (P.I.), R.W. Collins, V.G. Karpov,
Department of Physics and Astronomy,
Dean Giolando, Dept. of Chemistry
The University of Toledo
Toledo, OH 43606

This progress report covers the Second Quarter of Phase 3 for the period from September 01, 2007 through November 30, 2007, of the above Thin Film Photovoltaic Partnership Program subcontract. This report will present 1) results of Langmuir probe analysis of the plasma potential during RF magnetron sputtering, 2) recent results of high resolution electron microscopy studies of CdTe cells done in collaboration with the University of Michigan Electron Microbeam Analysis Laboratory, and 3) x-ray emission spectroscopy studies of sputtered CdS films and as-sputtered and $CdCl_2$-treated CdS/CdTe cell structures done in collaboration with the University of Nevada Las Vegas.

1 Potential Distribution During Magnetron Sputtering Deposition

1.1 Introduction

We reported previously that different deposition conditions such as sputtering gas pressure and applied RF power lead to differences in CdTe deposition rate, film morphology, surface roughness and residual stress. Consequently, cells grown under different conditions require some tweaking of the post-deposition treatment in order to achieve the best cell efficiency.

Additionally, we have observed that routine maintenance procedures such as CdTe target replacement and cleaning of the corresponding ground shield influence the deposition rate and the quality of the film. For example it has been found that the pinhole density reaches its maximum right after the cleaning of the ground shield and remains relatively high for a few subsequent depositions. On the other hand once a coating of CdTe is developed on the ground shield the pinhole density becomes vanishingly small although the deposition rate can slow by as much as 50% as the ground shroud coating builds up.

Not only does this present difficulties for maintaining a solid efficiency baseline throughout the sputtering target life cycle, it also reflects changes in the sputtering plasma. Being a plasma-assisted deposition technique, magnetron sputtering offers a wide range of tweaking opportunities to create thin films with desired physical properties. Without good understanding of the plasma processes the sputtering process can become excessively complicated.

The basic principles of magnetron sputtering are well known and readily available in the literature. It is important to apply those principles to a specific deposition process and equipment. In this report we provide the results of the potential distribution measurements done in one of the CdTe deposition chambers at the University of Toledo. This is the same chamber we recently reported the study of the deposition rate and the CdTe film morphology. These measurements of the plasma allow us to link the typical process control data from pressure gauges and power meters to the properties of the deposited film to potential distributions inside the chamber and plasma parameters extracted from the Langmuir probe measurements.

1.2 Experimental Setup

The experimental set up is sketched on the Figure 1.1. The magnetron sputter chamber has a planar geometry with an unbalanced magnetron. The distance between the 2” diameter CdTe target and the 3”x3”Tec-7 glass substrate is the 6.5 centimeters. The Langmuir probe made of a 10 mm long, 70 micron diameter Pt wire was placed in front of the center of the substrate 10 mm towards the CdTe target. 10 mm of wire protruded with the rest of the wire isolated from the plasma by the glass capillary tube and fed through the chamber wall for easy readout. We used a Keithley 2400 Sourcemeter to collect the I-V data. Two other feedthroughs were used for the substrate bias wire and target self-bias wire. The substrate holder was isolated from the chamber walls with a dielectric piece and normally during the deposition the substrate is kept at floating potential. The setup described above allowed us to measure the self-bias potential of the substrate as well as to apply a desired bias over the range of -50 to 50 V in order to check on the corresponding changes in plasma potential.

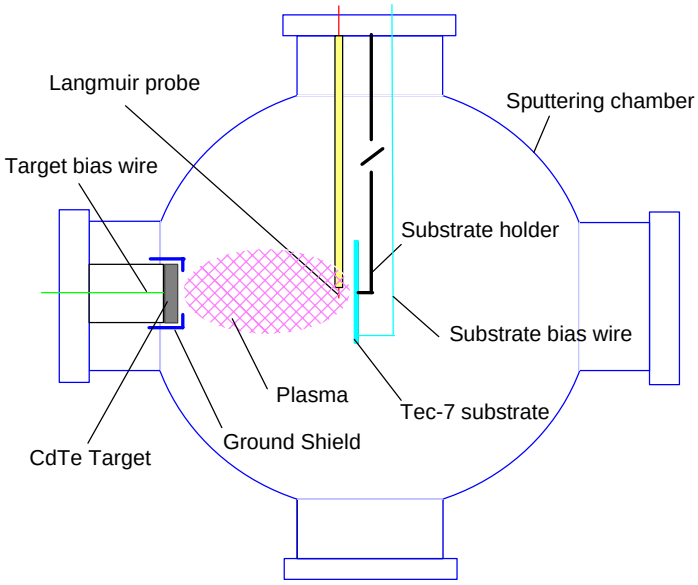

Figure 1.1. Experimental setup for potential distribution and the Langmuir probe measurements

In order to cover the most useful region in the phase space of deposition parameters we performed all the measurements for the Ar pressure range of 5 mTorr to 50 mTorr and RF power of 5 W to 60 W. In addition data were taken in two different configurations: with a fleshly cleaned ground shield (shroud) and a ground shield with a thick CdTe coating, equivalent to the coating that is normally built up after about 200 hours of deposition.

1.3 Cathode DC Bias

It is known that during RF sputtering the cathode (target) develops a certain negative DC bias. This happens as a result of the difference in mobilities of ions and electrons in the plasma. Assuming that before plasma breakdown the cathode was at ground DC potential with the RF signal was applied to it, after the plasma is ignited the ions from the plasma bombard the target in the negative half period causing sputtering. In the positive half period the electrons are attracted instead. After a few cycles due to the higher mobility of the electrons the target is found at added negative bias which is a function of both sputtering pressure and applied RF power as shown on the Figure 1.2.

The measured dependence of target self-bias on pressure is rather weak while it steadily becomes more and more negative when the RF power increases. Also there is a noticeable difference between clean and covered ground shield conditions – the cathode DC bias is always less negative for the same pressure and power conditions when the ground shield is covered with an insulating coating of CdTe.

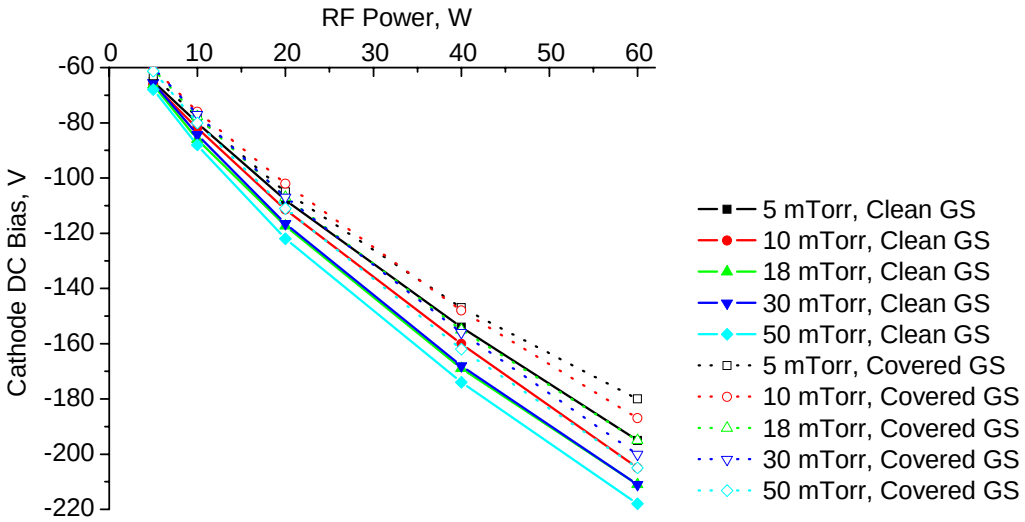

Figure 1.2. Cathode DC bias as a function of pressure and RF power. Clean ground (dot lines) and covered ground shield (solids)

1.4 Substrate Self-Bias

Our standard deposition configuration uses the substrate at floating bias. This is ensured by the dielectric insulation of the substrate holder. Therefore the substrate bias can change depending on the other deposition parameters. Here we measure that change for both clean and covered grounds shield conditions (Figure 1.3).

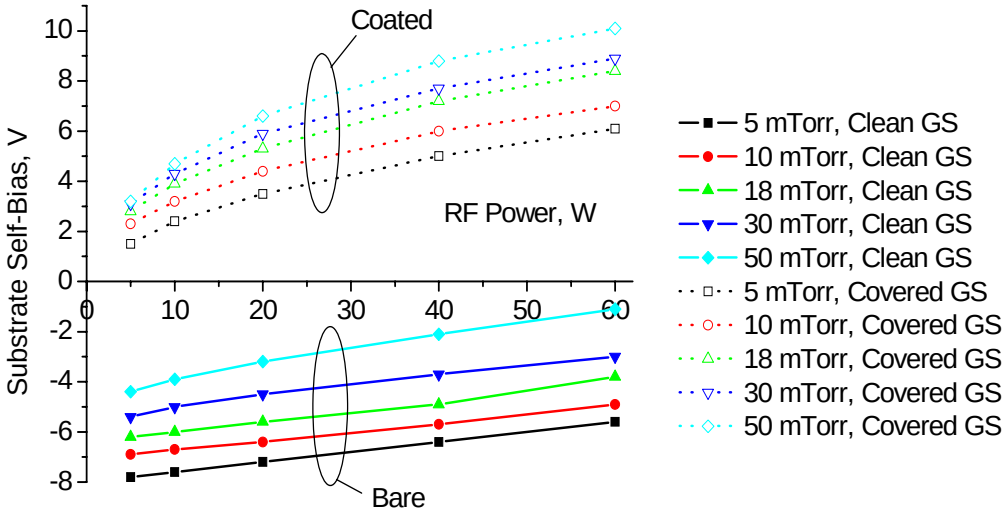

Figure 1.3 Substrate Self-Bias bias as a function of pressure and RF power. Clean ground (dot lines) and covered ground shield (solids)

As in the case of the cathode DC bias, the substrate self bias changes with both pressure and RF power. It becomes more positive (or less negative in some cases) when both pressure and power increase. We found the largest differences between the cases of clean and covered ground shield. We believe that it is important that for the case of a clean ground shroud the substrate is always found under negative self-bias while it eventually becomes positive when enough CdTe coating is developed on the shield. This can be an explanation for the observed change in pinhole density – extremely high right after the cleaning of the ground shield and subsiding later on as the total number of deposition hours increases. The exact cause is unknown but is consistent with the presence of positively charged dust particles inside the chamber that get attracted to the substrate when its self bias is negative and do not cause a problem otherwise. This hypothesis needs to be tested further.

1.5 Plasma Potential

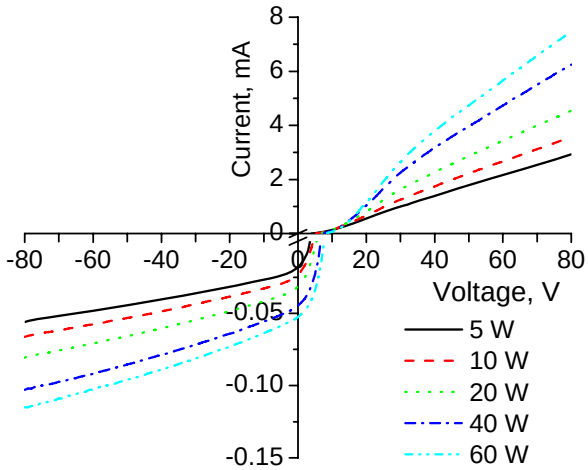

Figure 1.4 A typical set of I-V curves obtained with the Langmuir probe. Data taken with covered ground shroud at 18 mTorr

The plasma potential was determined from the analysis of the Langmuir probe trace which technically is an I-V curve taken over the range of -80 V to 80 V. A typical data set is presented i Figure 1.4. Figure 1.5 and Figure 1.6 illustrate the procedure for the analysis of the curve. First a straight line approximating the ion current is subtracted from the raw data (Figure 1.5).

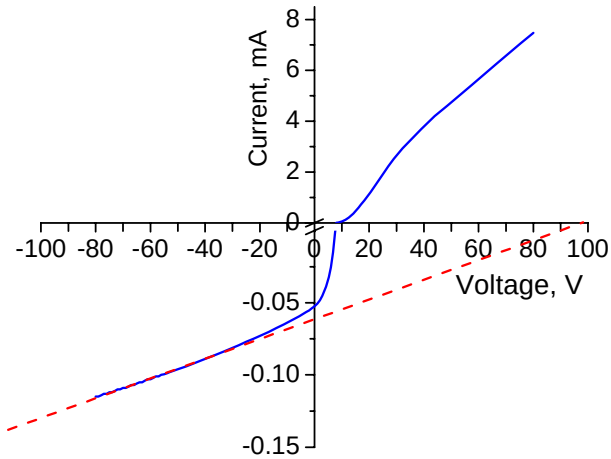

Figure 1.5 Subtraction of the ion current (red dashed line) from the raw data (blue solid line)

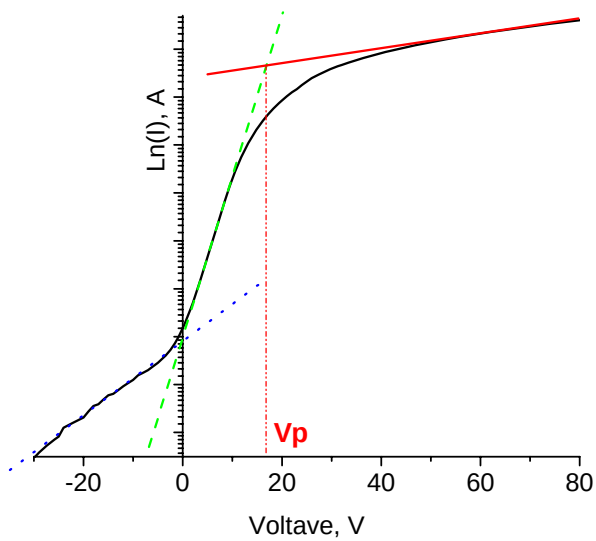

Figure 1.6 Langmuir probe trace evaluation

Second, the modified data are plotted on semi-logarithmic scale and the three distinct regions are approximated with straight lines. The red solid line on the Figure 1.6 is the approximation of the electron saturation current, the red dashed line represents the retardation region where the electron current increases rapidly and the blue dotted line represents the contribution from the high energy tail electrons. The plasma potential was determined by the intersection of the first two lines. The results are shown on the Figure 1.7.

In general it can be concluded that there is a very weak dependence of plasma potential on the RF power with a tendency to increase with increasing power while dependence on the sputtering gas pressure is rather unclear and likely to be within the experimental error. Again the largest difference is between the cases of covered and clean ground shields. The plasma potential is about 5 V higher in the case of the of covered ground shield.

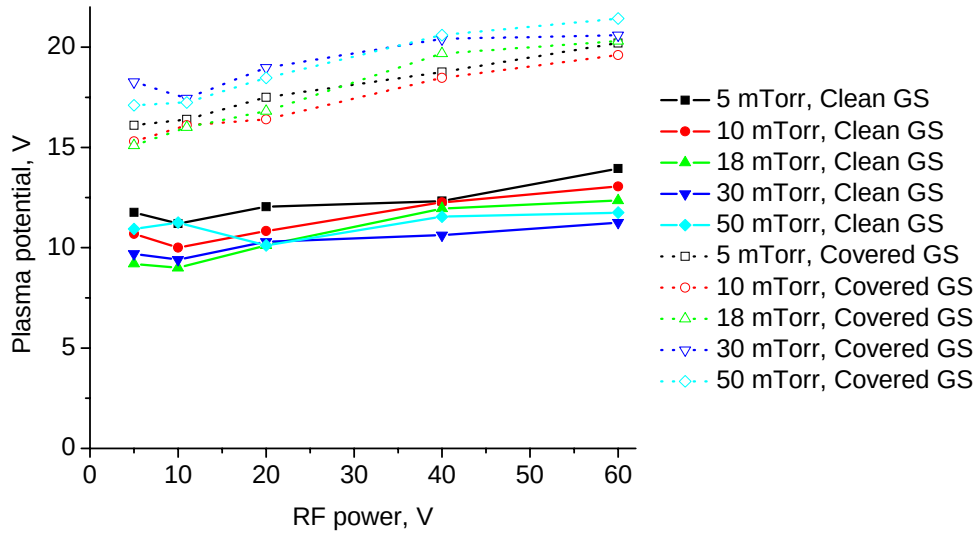

Figure 1.7 Plasma potential as a function of pressure and RF power. Clean ground shield (doted lines) and coated (covered) ground shield (solids)

1.6 Plasma potential vs. substrate bias

The final measurement of potential was done for the case of coated ground shield at 18 mTorr of Ar pressure and 20 W of RF power. The variable in this case was the substrate bias that was controlled by a DC power supply connected between the substrate (TEC-7 3”x3” glass) and the electric ground (chamber walls). We studied the evolution of the plasma potential while varying the substrate bias from -50 V to 50 V (Figure 1.8).

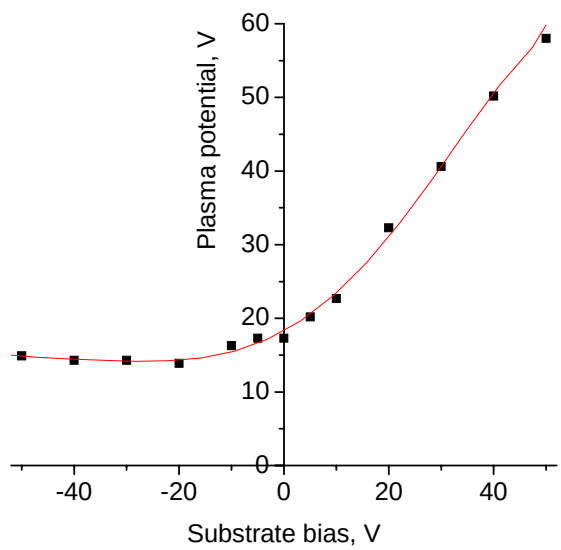

Figure 1.8 Plasma potential vs. applied substrate bias

It can be seen from the figure that the plasma potential is less sensitive to the application of the negative bias and very quickly reaches the constant value of about 14 V which is just slightly less that the plasma potential for the floating substrate bias condition (substrate self bias is about 4 V in this case). This can be explained by the low mobility of the ions and the fact that the plasma cannot be negative with respect to the chamber walls (0 V) regardless of the substrate bias. This limits the lowest possible potential the plasma can achieve. On the other hand, application of the positive substrate bias leads to the linear increase of the plasma potential since electrons are now easily drained from the plasma.

1.7 Conclusions

In this preliminary report on the Langmuir probe analysis of the potential inside the sputtering chamber provided measurements of the DC cathode bias, substrate self bias and plasma potential as functions of sputtering gas pressure and applied RF power. Although our results agree well with theoretical predictions and with some results that had been obtained before, we found a substantial difference between conditions resulting from using a freshly cleaned ground shield vs. one that had been in the chamber for about 100 hours of deposition.

This can explain the slowing down of the deposition rate that is observed as the CdTe coating on the ground shield builds up. A coated ground shroud results in a smaller potential difference between the plasma and the target DC bias that results in less integrated sputtering time over each RF cycle. This also provides a hint to understanding the phenomenon of a higher density of pinholes right after the cleaning of the ground shield. This procedure leads to the decrease of the substrate self bias by roughly 10 V which is enough to make it slightly negatively biased as opposed to the positive self bias which we believe typical for the major part of the target maintenance cycle.

It is also worth mentioning that we recently attempted to extend our typical 100 deposition hour ground shield cleaning cycle by 3 times and there were no other negative effects observed other than a decrease of the deposition rate. Instead high quality films with very low pinhole density yielding above 13% efficiency cells have been deposited.

Another important conclusion is that although our typical deposition parameters such as sputtering gas pressure and RF power are very useful for the process characterization and routine control, a periodic check on more fundamental quantities measured in this study is desirable and even might be necessary in certain cases such as full performance optimization, a major change in the manufacturing process, or a transition to new sputtering equipment.

2 Cross-sectional EDS mapping of sputtered CdTe solar cells

2.1 Introduction

As reported previously in Phase II (deliverable D.2.8 and D.2.2), we found both indirect and direct evidence indicating the existence of an interfacial Cu_2O layer between the CdTe and Au layers in our standard sputtered CdS/CdTe device. This evidence includes our fitting of EXAFS data from complete cell structures, the Z contrast of the HRTEM images at CdTe/Au interface and x-ray fluorescence collection of peeled off metal contacts. The thickness of such an interfacial Cu_2O layer is about 4Å and primarily in the chemical form of copper-oxide. A region of Cu:Au alloy is also found at the back contact with little Cu observable in the CdTe beyond 10 nm from the CdTe/Au

interface after forming our standard Cu(3nm)/Au(20nm) contact. Additional measurement by TEM as well as fine-probe EDS and electron energy loss spectroscopy (EELS) investigations on complete cell were planned in Phase III.

Here, we report our latest progress with cross-sectional, high-resolution high-angle annular dark field (HAADF) images and fine-probe EDS mapping on our standard cell through the collaboration with Kai Sun and the Electron Microbeam Analysis Laboratory (EMAL) at the University of Michigan.

We used a JEOL 3011 ultra-high resolution microscope (~0.17nm) and a JEOL 2010F analytical electron microscope that can be operated either in TEM or STEM mode (~0.17 nm). When performed in the STEM mode, a simultaneous atomic resolution HAADF image, i.e. Z-contrast imaging, can be obtained.

2.2 Sample Preparation

We fabricated CdS/CdTe devices by magnetron sputtering in a conventional structure on 3 mm TEC-7 glass. 0.13μm CdS and 2.2μm CdTe films were deposited without vacuum break followed by a 30 minute $CdCl_2$ vapor treatment with the temperature of sample at 397 °C and $CdCl_2$ source at 392 °C. As the next step, 40Å Cu and 200Å Au layers were evaporated on the top of the chloride treated films. The devices were then finished with a so-called "diffusion" process at 152 °C in ambient air for 52 minutes. The average performance of these cells is:

Eff = 11.9%, Voc = 800mV, Jsc = 20.7 mA/cm^2 and FF = 71.6%.

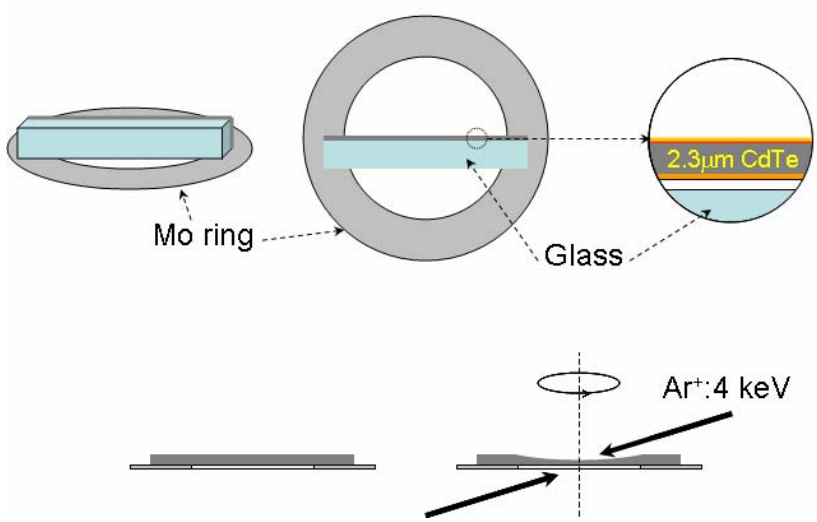

Figure 2.1 Steps of sample preparation for HRTEM.

Since the typical scattering volume of 300 keV (typical energy selected for ultra high resolution TEM scan) electrons in bulk CdTe is in the scale of *microns*, in order to obtain high resolution EDX mapping, a thinning process to reduce the sample thickness down electron transparency (typically 60-100nm) must be carried out. Figure 2.1 is an illustration of the thinning process. The preparation started by cutting the films on glass into a 1mm wide and 2.7mm long pieces, perpendicular to the film surface by a diamond disk saw. Then one side of the cut piece was attached by M-Bond onto a Mo ring with 3 mm diameter. Rough grinding was then carried out using grinding papers coated by Al_2O_3 powders with diameters of 30μm and 1μm, respectively. The sample is usually ground down to 100 μm before diamond power

dimpling under a rotating copper wheel, which will thin the sample further down to around several microns. The last step is performing ion milling at the center of the sandwich structure using a Gatan 691 Precision Ion Polishing System (PIPS™) performed at ~100 ºC. Two 4 keV Ar^+ beams with beam current about 15 μA are usually used at the early stage of milling. The two Ar^+ beams usually strike the upper and lower surfaces of the sample at a grazing angle of 4°. Once a small hole shows up, the ion beam voltage is reduced to about 3 kV and the final milling (polishing) is performed for about 10 minutes. Sample preparation was done mostly at the Univ. of Michigan.

2.3 Voids in CdTe Layer and at CdS/CdTe Interface

We collected both High-Angle Annular Dark-Field (HAADF) and scanning transmission electron microscopy bright field (STEM-BF) images on the same area of our sample as shown below in Figure 2.2. Apparent voids are observed in the 2.2 μm thick CdTe layer as the dark spots (low average Z number for electron diffraction) in Figure 2.2a and bright ones (means low mass density for electron transmission) in Figure 2.2b. These voids distribute in CdTe randomly with an approximate size of 0.3 μm. This is different from our previous results from the ellipsometry analysis of CdTe film grown on Si wafer, in which the void fraction increases with distance away from CdTe/Si interface (Deliverable D.1.7). Voids are also observed at the CdS/CdTe interface.

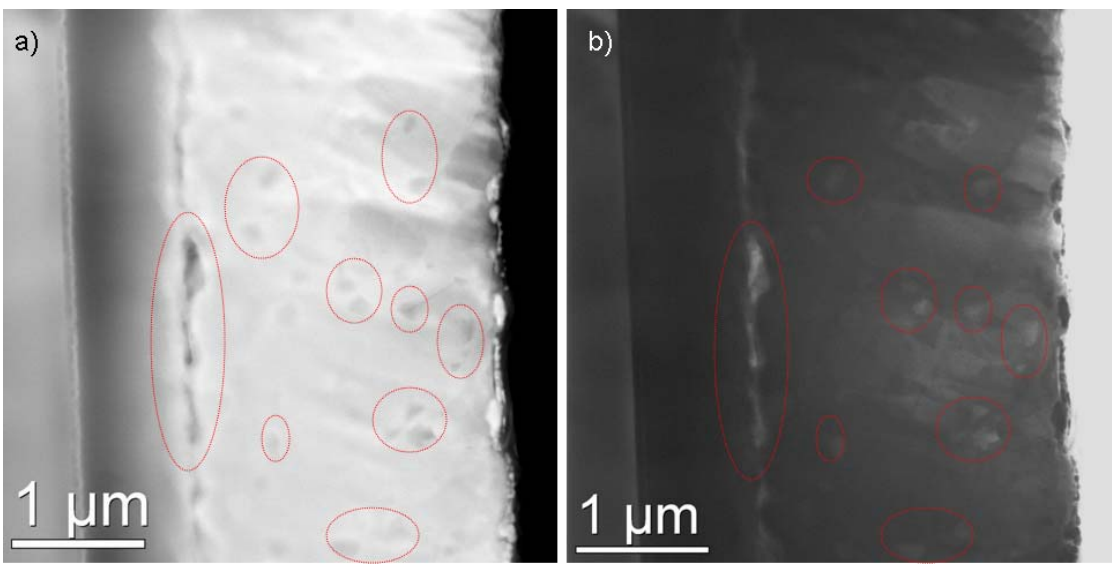

Figure 2.2 Cross-sectional (a) HAADF and (b) STEM-BF images of standard CdTe device. Voids are circled for emphasis.

EDX elemental mappings were obtained by collecting X-ray signals from the same cross-section area as Figure 2.2 to identify the distribution of the major elements in the sample from glass through TCO, CdS, CdTe and the back metal layer. The structure of which is labeled in the upper left inset of Figure 2.3 which is a tilted HAADF in low resolution. Other insets are the x-ray distribution maps of Cd, Te, S, Cu and Au. EDS mapping was performed in the STEM mode with an electron beam probe size 5 Å. The dimension of the x-ray emission area is usually less than 10 times of the probe size (normally 2~3 times).

The Cd and Te maps show relatively lower concentrations (dark spots as circled in Figure 2.3) of the both elements at the same locations as the dark spots in HAADF image (Figure 2.2 a). This confirms the existence of voids in CdTe layer. Low Cd concentration is also found at the CdS/CdTe interface which matches the locations of void segments in HAADF image.

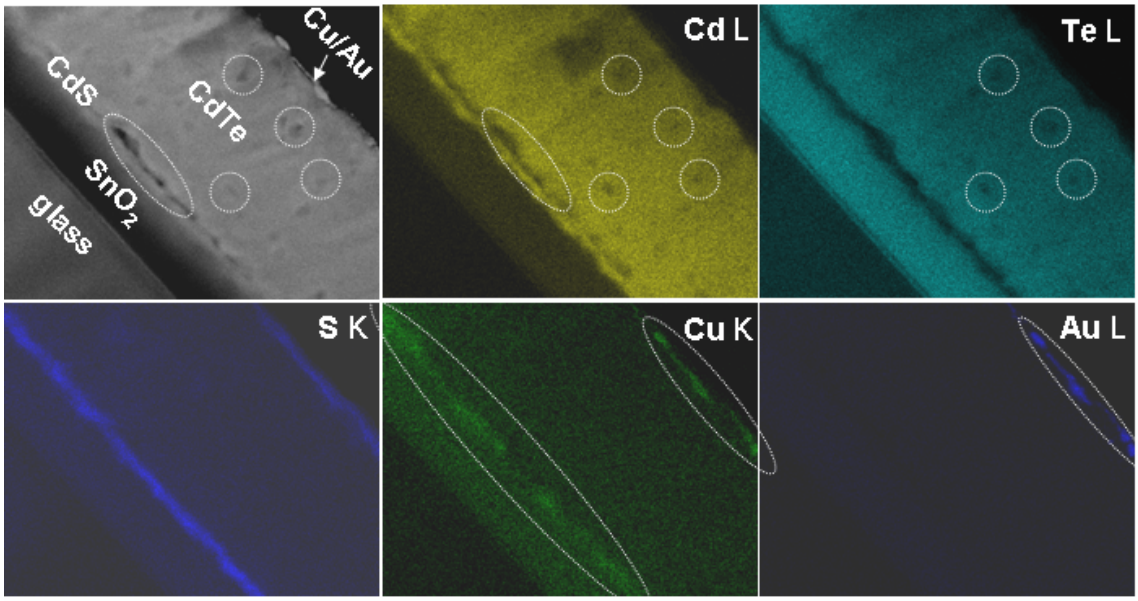

Figure 2.3 HAADF image and EDX mapping of Cd, Te, S, Cu and Au on the same area. The Te distribution appears in the area of SnO_2 layer is due to signal leakage of the Sn $L_{\beta 1}$ (3662.8 eV) peak into the Te $L_{\alpha 1}$ (3769.3 eV).

2.4 Cu in the metal contact and in CdS

A high concentration of Cu in the back metal contact layer is confirmed by this mapping (the two lower-right insets in Figure 2.3). Instead of being separated from the Au layer, Cu is found distributed in the same location as Au at the back contact. EDS mapping in other areas from the same sample confirms the same distribution area of Cu and Au at back contact (not shown). This indicates the formation of a Cu-Au alloy as suggested by our EXAFS theoretical fitting (deliverable D.2.8).

Another interesting feature is the relatively higher concentration of Cu in the CdS layer than in CdTe. We carefully compared the Cu mapping and HAADF image and found lower Cu concentration in the void segments at interface than in the CdS segments. This suggests some of the copper atoms diffuse from the back surface through the CdTe layer during back contact activation and accumulate in the CdS.

The Cu fluorescence signal from the SnO_2 (TCO) layer is also relatively stronger than from the CdTe layer but weaker than from CdS.

3. Sulfur Distribution at CdTe Back Surface and an XES study

Another significant feature indicated by the EDS mapping is the presence of some sulfur at the back surface of the CdTe. Besides the distribution with high concentration at the CdS layer, sulfur also distributes at the back surface around the interface between the CdTe and

Cu/Au. The thickness of the high sulfur concentration layer at the back surface is approximately 0.1μm. The sulfur concentration in this layer is much lower than in CdS but higher than in CdTe and SnO_2 as indicated by the different brightness. (See Fig. 2.3.)

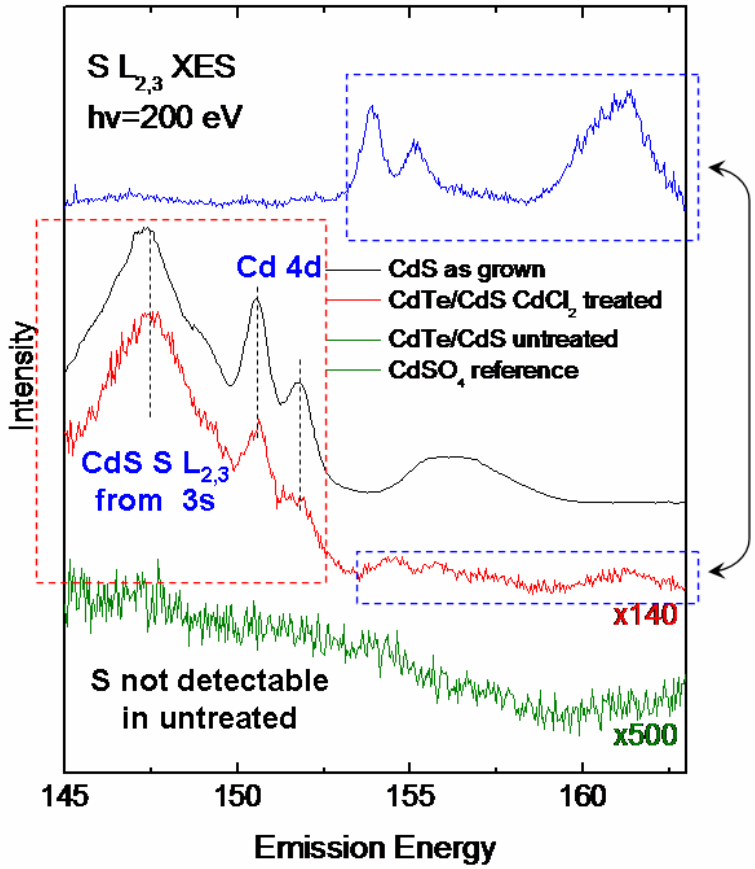

Figure 3.1 Sulfur $L_{2,3}$ XES spectra of as-grown CdS reference, as-grown and $CdCl_2$ treated CdTe/CdS, and a $CdSO_4$ (sulfate) reference. The spectrum of $CdCl_2$ treated CdTe/CdS is primarily comprised of CdS-like sulfur (as derived from the spectral shape below 153 eV) and sulfate-like sulfur (emission above 153 eV).

To understand the chemical form of this surface sulfur at CdTe back surface, we sent our standard sputtered CdS/CdTe films (0.13μm and 2.3μm, respectively) on TEC-7 together with as-grown CdS film (1.8μm) on fused silica to Lothar Weinhardt and Clemens Heske at the University of Nevada, Las Vegas for X-ray Emission Spectroscopy (XES) at the Advanced Light Source, Lawrence Berkeley National Lab. CdTe/CdS films both with and without standard vapor $CdCl_2$ treatment were studied. In S $L_{2,3}$ XES, sulfur 2p core holes are generated by an x-ray beam with energy of 200 eV and the emitted x-ray fluorescence is recorded (between 145 and 165 eV). The information depth of these studies is estimated to about 250 nm (http://www-cxro.lbl.gov/).

Figure 3.1 shows the S $L_{2,3}$ spectra for as-grown and chloride-treated CdTe/CdS films, an as-grown CdS film, and a $CdSO_4$ reference. While no S can be detected on the CdTe surface of the untreated CdTe/CdS/TEC-7 sample, we find a clear S $L_{2,3}$ signal in the range from 145 eV through 153 eV for the $CdCl_2$ treated sample, namely a dominant peak from S 3s states at approximately 148 eV and two sharp peaks just above 150 eV corresponding to the Cd 4d-derived bands. This signal is primarily comprised of CdS-like sulfur, as well as some sulfur in an oxidized (sulfate) environment. This can be seen by comparing the spectrum of the chloride-treated sample with a $CdSO_4$ reference in the energy range from 153 eV through 167 eV (with 140 times magnification).

Apparently, as a conclusion of our EDX mapping of sulfur and XES surface state study, the $CdCl_2$ treatment leads to S diffusion and accumulation at the back surface of CdTe and some of the diffused sulfur is oxidized to form a sulfate.